13. Tarucha, S., Austing, D. G., Honda, T., van der Haage, R. J. & Kouwenhoven, L. P. Shell filling and spin effects in a few electron quantum dot. *Phys. Rev. Lett.* **77,** 3613–3616 (1996).
14. Held, R. *et al.* In-plane gates and nanostructures fabricated by direct oxidation of semiconductor heterostructures with an atomic force microscope. *Appl. Phys. Lett.* **73,** 262–264 (1998).
15. Lüscher, S., Heinzel, T., Ensslin, K., Wegscheider, W. & Bichler, M. Signatures of spin pairing in a quantum dot in the Coulomb blockade regime. *Phys. Rev. Lett.* **86,** 2118–2121 (2001).
16. Heinzel, T. *et al.* Electronic properties of semiconductor nanostructures patterned by AFM lithography. *Physica E* **9,** 84–93 (2001).
17. Pedersen, S., Hansen, A. E., Kristensen, A., Sorensen, S. B. & Lindelof, P:. E. Observation of quantum asymmetry in an Aharonov-Bohm ring. *Phys. Rev. B* **61,** 5457–5460 (2000).
18. Cassé, M. *et al.* Temperature dependence of the Aharonov-Bohm oscillations and the energy spectrum in a single-mode ballistic ring. *Phys. Rev. B* **62,** 2624–2629 (2000).
19. Tan, W.-C. & Inkson, J. C. Electron states in a two-dimensional ring—an exactly soluble model. *Semicond. Sci. Technol.* **11,** 1635–1641 (1996).
20. Chakraborty, T. & Pietiläinen, P. Persistent currents in a quantum ring: Effects of impurities and interactions. *Phys. Rev. B* **52,** 1932–1935 (1995).
21. Kastner, M. A. The single-electron transistor. *Rev. Mod. Phys.* **64,** 849–858 (1992).
22. Berman, D., Entin-Wohlman, O. & Azbel, M. Y. Diamagnetic spectrum and oscillations in an elliptic shell. *Phys. Rev. B* **42,** 9299–9306 (1990).
23. Beenakker, C. W. J. Random-matrix theory of quantum transport. *Rev. Mod. Phys.* **69,** 731–808 (1997).
24. Schuster, R. & Ensslin, K. Antidot superlattices: classical chaos and quantum transport. *Adv. Solid State Phys.* **34,** 195–218 (1994).
25. Loss, D. & Goldbart, P. Period and amplitude halving in mesoscopic rings with spin. *Phys. Rev. B* **43,** 13762–13765 (1991).

Acknowledgements

We thank M. Büttiker and D. Loss for valuable discussions. Financial support from the Swiss Science Foundation (Schweizerischer Nationalfonds) is gratefully acknowledged.

Correspondence and requests for materials should be addressed to K.E. (e-mail: ensslin@phys.ethz.ch).

Coherent control of pulsed X-ray beams

M. F. DeCamp*, D. A. Reis*, P. H. Bucksbaum*, B. Adams†, J. M. Caraher*, R. Clarke*, C. W. S. Conover‡, E. M. Dufresne*, R. Merlin*, V. Stoica* & J. K. Wahlstrand*

* *Department of Physics and FOCUS Center, University of Michigan, Ann Arbor, Michigan 48109, USA*
† *Advanced Photon Source, Argonne National Labs, Argonne, Illinois 60439, USA*
‡ *Colby College, Waterville, Maine 04901, USA*

Synchrotrons produce continuous trains of closely spaced X-ray pulses. Application of such sources to the study of atomic-scale motion requires efficient modulation of these beams on time-scales ranging from nanoseconds to femtoseconds. However, ultrafast X-ray modulators are not generally available. Here we report efficient subnanosecond coherent switching of synchrotron beams by using acoustic pulses in a crystal to modulate the anomalous low-loss transmission of X-ray pulses. The acoustic excitation transfers energy between two X-ray beams in a time shorter than the synchrotron pulse width of about 100 ps. Gigahertz modulation of the diffracted X-rays is also observed. We report different geometric arrangements, such as a switch based on the collision of two counter-propagating acoustic pulses: this doubles the X-ray modulation frequency, and also provides a means of observing a localized transient strain inside an opaque material. We expect that these techniques could be scaled to produce subpicosecond pulses, through laser-generated coherent optical phonon modulation of X-ray diffraction in crystals. Such ultrafast capabilities have been demonstrated thus far only in laser-generated X-ray sources, or through the use of X-ray streak cameras[1–6].

X-ray anomalous transmission (the Borrmann effect) is a classical diffraction effect where X-rays propagate through a crystal with low loss over many average attenuation lengths[7–9]. The X-ray field found by solving Maxwell's equations in a periodic medium has two linearly independent eigensolutions (see Fig. 1). Solution α is the anomalous transmission wave, where absorption is reduced because the nodes of the X-ray field lie near the atomic crystal planes, as in a waveguide. Solution β has the antinodes of the field near the lattice planes, creating enhanced absorption. In crystals thicker than several attenuation lengths, the β-solution is almost completely absorbed, and the X-rays are nearly pure α-type. At the exit face of the crystal, the α-wave redistributes into two freely propagating X-ray beams with approximately equal intensities: the forward diffracted beam, with a momentum parallel to the original incident beam; and a deflected diffracted beam, which satisfies the Laue condition for a particular set of crystal planes.

Anomalous transmission is sensitive to small lattice distortions. Borrmann's own experiments demonstrated the sensitivity of anomalous transmission to lattice strain due to a small thermal gradient[10]. More recent work has shown that low-frequency acoustic waves can spatially modify the anomalous transmission[11] or even destroy it[12–14]. In all of these experiments, the induced strain weakens the anomalous transmission.

The forward and deflected beams are the eigenmodes outside the crystal. At the exit face of the crystal, α and β redistribute into orthogonal linear combinations of these two freely propagating mutually coherent X-ray beams. The α- and β-solutions propagate at different phase velocities, because they experience different indices of refraction. This leads to the Pendellösung effect—that is, the modulation of the intensity of the outgoing X-ray beams as a function of the total accumulated phase difference between the two interior solutions—provided that the crystal is thin enough for the β-solution not to be absorbed[7–9]. The key to coherent control of the X-ray pulses is to create coherent combinations of α and β near the exit face of the crystal, which will interfere to produce the desired modulation in the free solutions outside the crystal. In particular, a buried interface (such as a dislocation) repopulates the β-solution even after it has decayed away in a thick crystal[15].

In previous experiments on anomalous transmission[11–14], the perturbations encompassed the entire crystal bulk. In the present

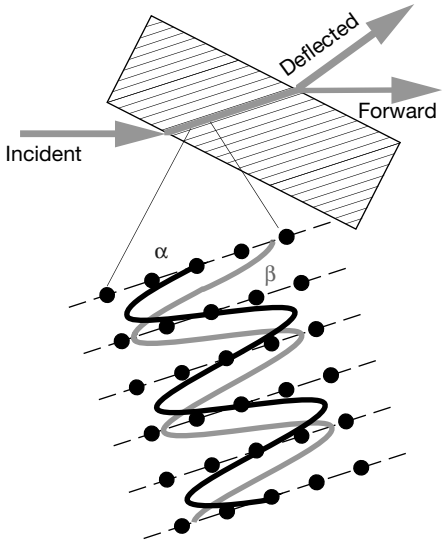

Figure 1 Geometry for X-ray diffraction from the asymmetric $\bar{2}02$ crystal planes of Ge[001]. Inside the crystal, the field consists of two transverse standing waves: the α-wave has its nodes on the atomic planes and thus experiences low absorption, while the β-wave has its antinodes on the atomic planes and thus experiences enhanced absorption. At the exit face of the crystal, α and β redistribute into orthogonal linear combinations of two freely propagating X-ray beams: a forward-diffracted beam and a deflected-diffracted beam.

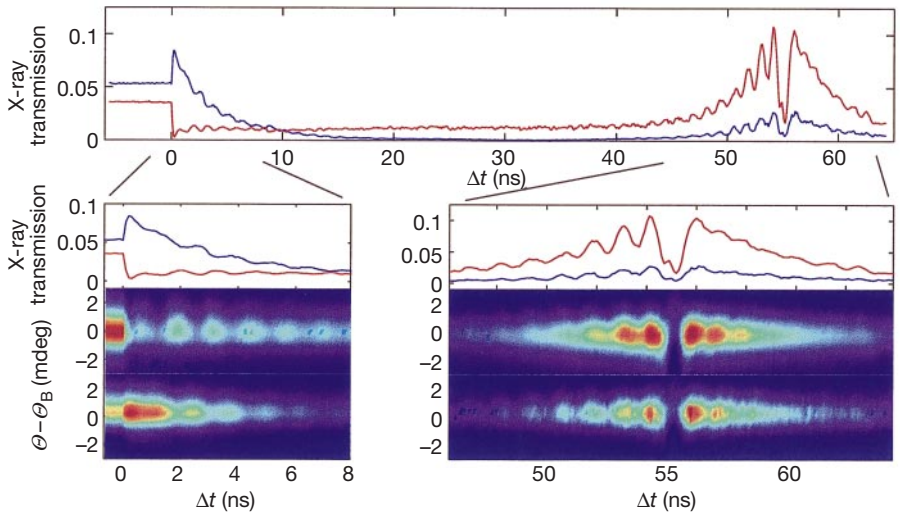

Figure 2 Time-resolved measurement of the $\bar{2}02$ diffraction following laser impulsive excitation of an acoustic wave on the exit face of a thick Ge [001] crystal. Top: forward (blue) and deflected (red) X-ray intensity near the diffraction peak as a function of time delay (Δt) following excitation. Bottom: expanded scale showing the regions where the acoustic pulse is near the exit or entrance crystal surface. Two-dimensional plots: the measured X-ray transmission versus Δt and crystal angle ($\Theta - \Theta_B$) near the forward (top) and deflected (bottom) diffraction peaks in normalized false colour.

work, an ultrafast (70-fs) laser pulse is absorbed in a 200-nm-thick surface layer of a 280-μm-thick Ge single crystal. This launches an acoustic impulse into the crystal[16–20], which modulates the ratio of the two diffracted X-ray beams on a subnanosecond timescale. The laser absorption, and the accompanying acoustic impulse, occurs over a length much less than the characteristic Pendellösung length (~5 μm). The impulse can be modelled as a thin interface that separates two distinct but otherwise perfect crystals. This interface rotates the wave solution in the (α,β) basis (thus maintaining their mutual coherence), in effect modifying the boundary conditions to the second crystal. By adjusting the delay between the X-rays and the acoustic pulse we can cause the exit beams to switch energy preferentially from one beam to another, modulate the two beams together, or even enhance the anomalous transmission.

The experiments were performed at the Michigan-Howard-Lucent Technologies undulator beamline at the Advanced Photon Source synchrotron. The spacing between X-ray pulses was 152 ns, sufficient to detect single X-ray pulses by gating the signal from a silicon avalanche photodiode (APD). Two independent APDs were used to measure the forward and deflected beams simultaneously. A Si(111) double crystal monochromator delivered up to 10^7 10-keV X-ray photons per pulse in a bandwidth of 1.4 eV. The X-ray switch was a 280-μm crystal of Ge[001], polished on both faces, which was impulsively excited by a 70-fs laser pulse, at 840 nm wavelength, with a fluence of ~5 mJ cm^{-2}. The X-ray attenuation length at 10 keV is 50 μm. The laser was synchronized to the X-ray pulses with a precision of 19 ps, over a delay of −1 to 1 ms. Our measurement resolution was limited by the X-ray pulse length of ~100 ps.

Figure 1 illustrates the transmission geometry for X-rays incident in a direction that satisfies the Bragg condition for the $\bar{2}02$ crystal planes of a [001]-oriented crystal. This geometry is asymmetric, in that the forward and deflected beams leave the crystal at different angles with respect to the surface normal. Inside the crystal, the X-rays propagate at 45° with respect to the surface normal, parallel to the crystal planes, such that the effective propagation distance was about eight average attenuation lengths. Figure 2 shows the time-resolved transmission following ultrafast laser-excitation on the exit face of the crystal (the face at which the α- and β-solutions redistribute into the freely propagating forward and deflected beams). We detected both the forward and the deflected X-rays as a function Δt and as a function of crystal angle, near the diffraction peak. (Δt is the time difference between the arrival of the X-ray pulse and the laser pulse; the deviation from the Bragg condition is given by $\Theta - \Theta_B$.)

At time delays less than $\Delta t = 0$, the X-rays arrive at the crystal before any laser excitation, and propagate via the Borrmann effect. The incident beam outside the crystal splits into α and β immediately inside the surface, and because the crystal is thick, only the α portion propagates with little attenuation. At the output face, α splits into approximately equal portions of forward and deflected beam.

Starting at $\Delta t = 0$, the diffracted intensity switches from the deflected beam to the forward beam. Approximately 75% of the energy is transferred in less than 100 ps. The amount of energy transfer was observed to depend on the incident laser fluence. As only the α-solution exists at the exit face, a full transfer of energy requires repopulation of the β solution. After X-ray propagation over one-quarter of a Pendellösung period (which is greater than 1.25 μm for 10-keV X-rays in this geometry), the output has switched to pure forward or deflected X-rays, depending on the initial sign of the rotation. Assuming an upper limit of the switch time given by our resolution of 100 ps, this implies that either the Pendellösung length decreases by a factor of at least 2.5 or the excitation propagates into the crystal at greater than 2.5 times the sound speed (5,000 m s^{-1} for longitudinal acoustic phonons along [001]). To resolve the initial switch mechanism, faster time resolution (for example a picosecond X-ray streak camera) may be required.

The Pendellösung length decreases as the crystal tilts away from the Laue resonance. A transient strain with components along the reciprocal lattice vector could reduce the oscillation length enough to switch the beams. Another possible mechanism is the supersonic transfer of energy through the ambipolar diffusion of the dense electron–hole plasma produced by laser excitation. The plasma then provides the source of stress that produces lattice strain in the crystal[17,21,22]. Estimates based on our experimental parameters indicate that either mechanism is plausible.

Following the initial switch in Fig. 2, Pendellösung oscillations are apparent in both the forward and deflected beams. The oscillations appear to be π radians out of phase with a frequency of ~1 GHz. This frequency is consistent with the passage of an acoustic impulse that redistributes energy from the α wave to a linear combination of α and β as it moves along the [001] crystal normal at the speed of sound. These oscillations decay with a time constant ~5 ns. This is

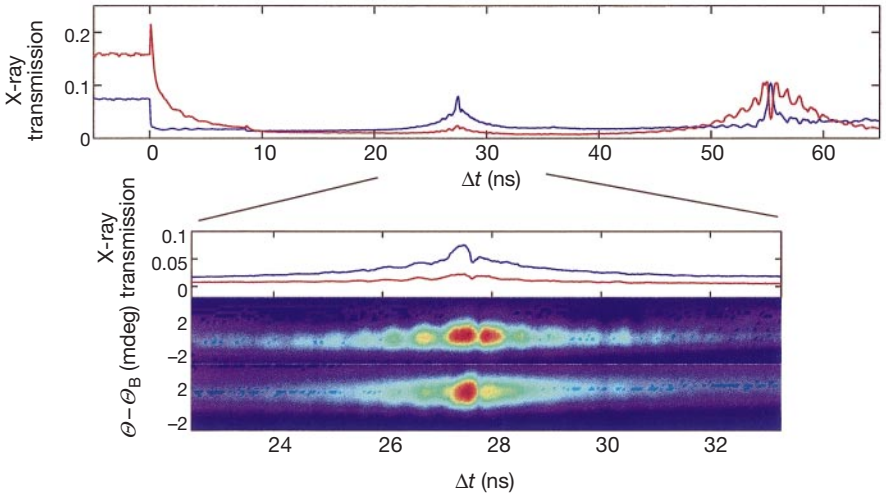

Figure 3 Time-resolved measurement of the $20\overline{2}$ diffraction following simultaneous impulsive excitation of an acoustic wave on the entrance and exit faces of a thick Ge[001] crystal. Top: forward (blue) and deflected (red) X-ray intensity near the diffraction peak as a function of time delay (Δt) following excitation. Bottom: expanded scale showing the region where the two acoustic pulses cross in the centre of the crystal. Two-dimensional plots: the measured X-ray transmission versus Δt and crystal angle ($\Theta - \Theta_B$) near the forward (top) and deflected (bottom) diffraction peaks in normalized false colour.

faster than an average attenuation length divided by the speed of sound (~10 ns), owing to the enhanced absorption of the β solution.

Around 55 ns the acoustic pulse approaches the input face of the crystal at the sound speed, so that the acoustic disturbance forms a thin interface separating the near-input region from the rest of the crystal. The diffraction efficiency increases as the interface approaches the input face because the initial β solution has not yet decayed. Once again, the time constant is determined by the β absorption and the speed of sound. The disturbance is such that the rotation of the (α,β) basis results in an increased amplitude in the α solution. Pendellösung oscillations are apparent as the interface moves through the crystal in this near-surface region. However, the two diffracted beams now oscillate in phase because the β solution is severely attenuated by the following thick crystal; that is, the two external fields are determined solely by the α-solution (anomalous transmission) as it is modified at the interface.

We can double the Pendellösung frequency by colliding two counter-propagating acoustic disturbances. Figure 3 shows the X-ray transmission in the forward and deflected beams following simultaneous excitation of acoustic waves on the input and output crystal faces. In this case the crystal was oriented so that the incident wave diffracts from the $20\overline{2}$ planes. This is similar to the $\overline{2}02$ geometry (Fig. 1) except that the incident beam is now along a direction parallel to the $\overline{2}02$ deflected beam, that is, the opposite asymmetry.

Two acoustic pulses separate the crystal into three regions. Near $\Delta t = 0$ and again near $\Delta t = 55$ ns a thick inner crystal is separated by thinner crystals at the entrance and exit faces. The initial switch increases the intensity of the deflected beam and decreases the intensity in the forward beam. This is in contrast to the effect observed with the switch using the opposite asymmetry. We also observed (not shown) that single-pulse excitation in this geometry results in a similar initial redistribution of energy. We infer that the sign of α/β at the point of the disturbance changes with the crystal orientation asymmetry. Near $\Delta t = 27.5$ ns, or half of the acoustic transit time, a thin crystal develops in the centre of the Ge. This is accompanied by a revival of the Borrmann effect that is particularly evident in the deflected beam. Pendellösung oscillations are again visible but the oscillation frequency is now ~2 GHz, indicating that two interfaces are approaching each other at twice the speed of sound. As Δt approaches 55 ns, the oscillations are out of phase because the β-solution is repopulated by the acoustic pulse launched from the input surface at $\Delta t = 0$.

We have created an efficient X-ray switch that can transfer energy between two widely separated X-ray beams at speeds faster than 100 ps. The motion of atoms in the crystal lattice limits the ultimate speed of this switch. Optical phonon excitations in this geometry could lead to subpicosecond switching times. □

Received 13 June; accepted 3 September 2001.

1. Kieffer, J.-C. *et al.* Ultrafast X-ray sources. *Phys. Fluids B* **5,** 2676–2681 (1993).
2. Rousse, A. *et al.* Efficient Kα x-ray source from femtosecond laser-produced plasmas. *Phys. Rev. E* **50,** 2200–2207 (1994).
3. Murnane, M. M. *et al.* Ultrafast X-ray pulses from laser-produced plasmas. *Science* **251,** 531–536 (1991).
4. Schoenlein, R. W. *et al.* Femtosecond X-ray pulses at 0.4Å generated by Thomson scattering: A tool for probing the structural dynamics of materials. *Science* **274,** 236–238 (1996).
5. Schoenlein, R. W. *et al.* Generation of femtosecond pulses of synchrotron radiation. *Science* **287,** 2237–2240 (2000).
6. Larsson, J. *et al.* Ultrafast x-ray diffraction using a streak-camera detector in averaging mode. *Opt. Lett.* **22,** 1012–1014 (1997).
7. Batterman, B. & Cole, H. Dynamical diffraction of X rays by perfect crystals. *Rev. Mod. Phys.* **36,** 681–716 (1964).
8. Warren, B. E. *X-Ray Diffraction* (Dover, New York, 1990).
9. Zachariasen, W. H. *Theory of X-ray Diffraction in Crystals* (Wiley and Sons, New York, 1945).
10. Borrmann, G. & Hildebrandt, G. Rontgen-Wellenfelder in Grossen Kalkspatkristallen und die Wirkung Einer Deformation. *Z. Naturforsch. A* **11,** 585–587 (1956).
11. Hauer, A. & Burns, S. J. Observation of an x-ray shuttering mechanism utilizing acoustic interruption of the Borrmann effect. *Appl. Phys. Lett.* **27,** 524–526 (1975).
12. Entin, I. R. *et al.* X-ray acoustic resonance in a perfect silicon crystal. *Sov. Phys. Solid State* **20,** 754–756 (1978).
13. LeRoux, S. D., Colella, R. & Bray, R. X-ray diffraction studies of acoustoelectrically amplified phonon beams. *Phys. Rev. Lett.* **35,** 230–234 (1975).
14. Chapman, L. D., Colella, R. & Bray, R. X-ray diffraction studies of acoustoelectrically amplified phonons. *Phys. Rev. B* **27,** 2264–2277 (1983).
15. Authier, A., Lagomarsino, S. & Tanner, B. K. (eds) *X-ray and Neutron Dynamical Diffraction, Theory and Applications* (Plenum, New York, 1996).
16. Thomsen, C. *et al.* Surface generation and detection of phonons by picosecond light pulses. *Phys. Rev. B* **34,** 4129–4138 (1986).
17. Akhmanov, S. A. & Gusev, V. E. Laser excitation of ultrashort acoustic pulses: new possibilities in solid-state spectroscopy, diagnostics of fast processes, and nonlinear acoustics. *Sov. Phys. Usp.* **35,** 153–191 (1992).
18. Rose-Petruck, C. *et al.* Picosecond-milliangstrom lattice dynamics measured by ultrafast X-ray diffraction. *Nature* **398,** 310–312 (1999).
19. Lindenberg, A. *et al.* Time-resolved X-ray diffraction from coherent phonons during a laser induced phase transition. *Phys. Rev. Lett.* **84,** 111–114 (2000).
20. Reis, D. A. *et al.* Probing impulsive strain with X-ray pulses. *Phys. Rev. Lett.* **86,** 3072–3075 (2001).
21. Auston, D. H. & Shank, C. V. Picosecond ellipsometry of transient electron-hole plasmas in germanium. *Phys. Rev. Lett.* **32,** 1120–1123 (1974).
22. Young, J. F. & van Driel, H. M. Ambipolar diffusion of high-density electrons and holes in Ge, Si, and GaAs: many-body effects. *Phys. Rev. B* **26,** 2147–2158 (1982).

Acknowledgements

We thank R. Colella and J. Wark for discussions, and D. Arms for technical support. This work was conducted at the MHATT-CAT insertion device beamline at the Advanced Photon Source. Use of the Advanced Photon Source was supported by the US Department of Energy Basic Energy Sciences, Office of Energy Research. We also acknowledge partial support from the National Science Foundation, the Center for Ultrafast Optical Science, and the AFOSR through the MURI programme.

Correspondence and requests for materials should be addressed to M.F.D. (e-mail: mattydee@umich.edu).

Spin-dependent exciton formation in π-conjugated compounds

J. S. Wilson*, A. S. Dhoot*, A. J. A. B. Seeley*, M. S. Khan†, A. Köhler* & R. H. Friend*

* *Cavendish Laboratory, Madingley Road, Cambridge, CB3 0HE, UK*
† *Department of Chemistry, Sultan Qaboos University, Al-Khod 123, Oman*

The efficiency of light-emitting diodes (LEDs) made from organic semiconductors is determined by the fraction of injected electrons and holes that recombine to form emissive spin-singlet states rather than non-emissive spin-triplet states. If the process by which these states form is spin-independent, the maximum efficiency of organic LEDs will be limited to 25 per cent[1]. But recent reports have indicated fractions of emissive singlet states ranging from 22 to 63 per cent[2–5], and the reason for this variation remains unclear. Here we determine the absolute fraction of singlet states generated in a platinum-containing conjugated polymer and its corresponding monomer. The spin-orbit coupling introduced by the platinum atom allows triplet-state emission, so optically and electrically generated luminescence from both singlet and triplet states can be compared directly. We find an average singlet generation fraction of 22 ± 1 per cent for the monomer, but 57 ± 4 per cent for the polymer. This suggests that recombination is spin-independent for the monomer, but that a spin-dependent process, favouring singlet formation, is effective in the polymer. We suggest that this process is a consequence of the exchange interaction, which will operate on overlapping electron and hole wavefunctions on the same polymer chain at their capture radius.

Several sophisticated methods have been used to determine the singlet generation fraction in organic LEDs, but these are often complicated by the fact that triplet states are generally non-emissive in conjugated organic compounds. As a result it has previously only been possible to place a lower limit on the singlet generation fraction in polymer LEDs. We have circumvented the problem of a non-emissive triplet state by investigating a Pt-containing polymer and its corresponding monomer (Fig. 1). The heavy Pt atom introduces spin-orbit coupling which allows the spin of the electron to flip or rephase and transitions between the singlet and triplet manifolds become possible[6]. Conjugation is preserved through the Pt atom by mixing of the frontier orbitals of the Pt and the ligand[7]. Direct emission from the triplet state is therefore observed for both optical and electrical excitation of LEDs made from these materials and this allows a straightforward calculation of the absolute singlet generation fraction.

The photoluminescence and electroluminescence spectra of the polymer and monomer (Fig. 2) both show two characteristic emission bands, and the relative contribution of each band to the total emission is indicated as a percentage. The high and low energy bands are due to singlet and triplet excited states S_1 and T_1, respectively. The triplet-state emission of this polymer and monomer and that of other similar materials has been well characterized previously by lifetime and photoinduced absorption measurements[8–11]. The triplet emission is observed at around 0.7 eV below the singlet in this and other conjugated polymers[9,10,12–14] and this finite exchange energy implies an excited state which is self-localized.

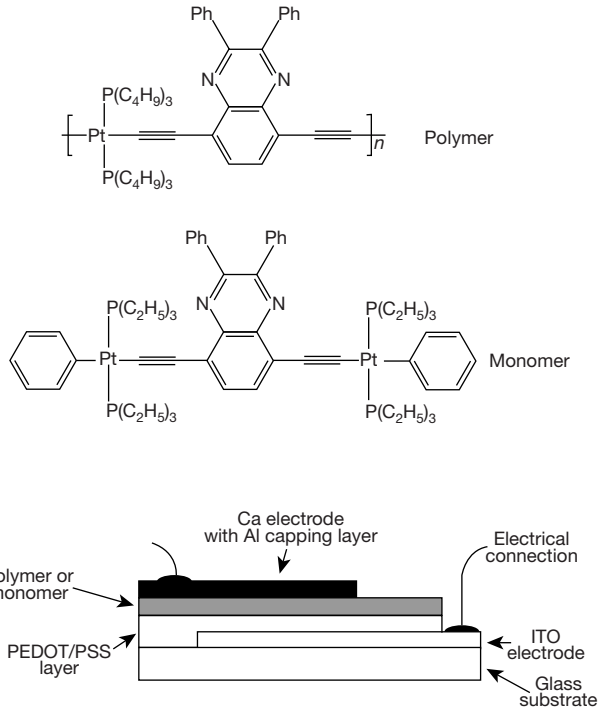

Figure 1 The chemical structures of the platinum-containing polymer and monomer investigated. A schematic of the simple light-emitting diode structure used is also given. PEDOT, poly(3,4-ethylenedioxythiophene); PSS, poly(styrenesulphonate); ITO, indium-tin oxide.

We note that although the spin-orbit coupling induced by the heavy Pt atom has been shown to produce close to 100% intersystem crossing[8] from the S_1 state to T_1, there is still more emission observed from S_1 than from T_1 in photoluminescence at 290 K. This is because, despite the T_1–S_0 transition being partially allowed in this polymer and monomer, the radiative decay rates from the triplet states are still only of the order of $10^3\,s^{-1}$ in comparison with non-radiative decay rates of 10^6–$10^5\,s^{-1}$, so only one in 1,000 of the triplets generated emits[15]. The non-radiative decay rate increases exponentially with decreasing T_1–S_0 gap and is controlled by multi-phonon emission[15].

In order to compare electroluminescence and photoluminescence spectra we measured both in LED structures. For electrical excitation we observe a greater percentage of the photons to be from the triplet state than with optical excitation, but in other respects the spectra are very similar (Fig. 2). In order to use the emission spectra to calculate the fraction of excited states generated in the singlet spin state, χ_S, we model the processes of photoluminescence and electroluminescence as shown in Fig. 3. In photoluminescence a number I of excitons are originally all created in the singlet S_1 state, and from there they decay radiatively (with a decay rate $k_{R(S)}$) or non-radiatively (with a decay rate $k_{NR(S)}$) to the singlet ground state S_0, or undergo intersystem crossing to the triplet manifold (with a rate k_{ISC}). Both radiative and non-radiative decay occurs from the triplet state T_1 to the ground state S_0. For electroluminescence the processes are exactly the same as in photoluminescence, with the important exception that it is also possible to create a fraction χ_T of triplet excitons directly. We define the quantum yields